Supporting Information

Buried and Bulk Synergistic Engineering Enable High-Performance Inverted 2D/3D Perovskite Solar Cells

Zonglong Song,[‡a] Yu Zou,[‡a] Yuping Gao,[a] Xingbang Gao,[a] Liu Yang,[d] Hang Liu,[a] Yuting Ma,[a] Rui Wang,[a] Ziyang Hu,[d] Yongsheng Chen,[a,b] Baomin Xu,*[c] and Yongsheng Liu*[a,b]

[a]The Centre of Nanoscale Science Technology, Key Laboratory of Functional Polymer Materials (Ministry of Education), Frontiers Science Center for New Organic Matter (Ministry of Education), College of Chemistry, Nankai University, Tianjin 300071, China. E-mail: liuys@nankai.edu.cn

[b]Haihe Laboratory of Sustainable Chemical Transformations, Tianjin 300192, China

[c]Department of Materials Science and Engineering, SUSTech Energy Institute for Carbon Neutrality, Southern University of Science and Technology, Shenzhen 518055, China
E-mail: xubm@sustech.edu.cn

[d]Department of Microelectronic Science and Engineering, School of Physical Science and Technology, Ningbo University, Ningbo 315211, China

1. Materials

N, N-dimethylformamide (DMF) (99.8%,Alfa Aesar), bathocuproine (BCP), PbI_2 (99.99%, TCI), The nickel nitrate hexahydrate ($Ni(NO_3)_2{\cdot}6H_2O$, 99.999%), sodium hydroxide (NaOH, 99.9%), Chlorobenzene (99.9%), 4,4-Difluoropiperidinehydrochloride (Aladdin). NiO_x nanoparticles (NPs), PCBM (Advanced Election Technology). Cesium iodide (CsI, 99.99%), Methylammonium chloride (MACl, 99.5%), C60 (99.9%), Lead bromide ($PbBr_2$, 99.99%) and Piperazinium iodide (PI, 99.5%) were bought from Xi'an Yuri Solar. $FAPbI_3$, $MAPbI_3$, $CsPbI_3$ microcrystals were synthesized as previous work[1]. *N,N*-dimethylformamide (DMF, 99.5%), dimethyl sulfoxide (DMSO, 99.5%), chlorobenzene (CB, 99.5 %), and isopropanol (IPA, 99.5%) were purchased from J&K.

2. Method

2.1 Preparation of 3D Perovskite Precursor Solution

$Cs_{0.05}FA_{0.85}MA_{0.1}PbI_3$ device: The ITO glass (12-15 Ω sq^{-1}; 1.5 × 1.5 cm^2 for a regular device) was progressively washed by cleaned with DI-water, acetone and isopropanol, each for 15 minutes in an ultrasonic bath. The cleaned ITO substrates were subjected to ultraviolet–ozone for 25 min (FHR UVOH 150 Lab). The single-junction cell configuration is ITO/NiO_x/Perovskite/PCBM/BCP/Ag. A thin layer of NiO_x (20mg/mL, DI water) was spin-coated onto glass/ITO at 5000 rpm for 30 s and annealed at 150 °C for 10 min. After transfer the substrates into an N_2-filled glovebox. 100 μL of FuMACl was then spread on the substrate with the rpm of 5000r/30s, then annealed at 100 °C for 5 min as target-1. 1.63 M perovskite precursor solution was prepared by mixing $FAPbI_3$, $MAPbI_3$, $CsPbI_3$ microcrystals with the molar ratio of 0.85: 0.1: 0.05 and additional 10 mol% MACl was added in mixed solvents of DMF:DMSO = 4:1 (vol/vol). The solution was stirred at room temperature for 2 h before use. $(4,4\text{-DFP})_2PbI_4$ crystal seed was added in control solutions with a concentration of 0.5 mg/mL as target-2 solutions. 100 μL of perovskite solution was then spread on the substrate and spun using one step spin-coating process (2000 rpm for 10 s, 5000 rpm/30s). 10-13 s before the end of the program, 300 μL of CB as the anti-solvent was dripped on the film. The films were then annealed at 110 °C for 15 min. After cooling to room temperature, 60 μL PI solution (0.5 mg mL^{-1} in IPA) was spin-coated onto the perovskite film as passivation layer at 5000 rpm for 30 s, followed by annealing at 100 °C for 5 min. Following this, the $PC_{61}BM$ (20mg/mL, CB) acting was spin-coated on the perovskite film at 1200 rpm for 30 s. The BCP (0.6 mg/mL, IPA) solution was spin-coated on $PC_{61}BM$ film at 1000 rpm for 30 s. Finally, a 100 nm thick Ag layer was thermally deposited on the substrate under high vacuum.

Mini-module fabrication: The deposition steps before the hole transport layer are consistent with those of small area devices, and the hole transport layer and electrode were completed by thermally evaporating C60 (40 nm), BCP (4 nm) and 100 nm Ag below 1×10^{-5} torr. For the scribing process, the ITO substrate was first etched by a laser scriber to form P1 lines. The P2 lines were etched after depositing BCP by mechanical scribing. The P3 lines were etched after silver deposition by mechanical scribing. The 5 cm× 5 cm ITO substrate displayed an active area of 10.80 cm^2 with 6 subcells.

WBG Perovskite: The perovskite was prepared following the typical triple cation process. In short, 1.5 M nominal PbI_2 and FAI in DMF: DMSO = 4:1 volume was first prepared as stock solutions (shaken overnight at 60 °C), and 1M $MAPbBr_3$ prepared by MABr and $PbBr_2$ also

shaken overnight at 60 °C. The so obtained $FAPbI_3$ and $MAPbBr_3$ were then mixed in 55:45. Finally, 5 vol % of 1.5 M nominal CsI in DMSO was added to the perovskite precursor. 100 µl of perovskite solution was then spread on the substrate and spun using one step spin-coating process (3500 for 35 s, 5 s acceleration). 10-13 s before the end of the program, 300 µl of CB the anti-solvent was dripped on the film. The films were then annealed at 100 °C for 15-30 min. After cooling to room temperature, 60 µL PI solution (0.5 mg mL^{-1} in IPA) was spin-coated onto the perovskite film as passivation layer at 5000 rpm for 30 s, followed by annealing at 100 °C for 5 min.

3. Measurements

^1H NMR spectra were measured by Bruker AV400 Spectrometer. X-ray photoelectron spectroscopy (XPS) measurements and ultraviolet photoelectron spectroscopic (UPS) were conducted by Thermo ESCALAB 250XI. UV-vis absorption spectra of perovskite films were performed by Cary 5000 UV-visible-NIR spectrophotometer. Photoluminescence (PL), temperature-dependent PL and time-resolved photoluminescence (TRPL) were obtained by FLS1000, Edinburgh Instruments Ltd with excitation at 450 nm. The perovskite films were deposited on non-conductive glasses. X-ray diffractions (XRD) data were measured by a Rigaku Ultima IV X-ray powder diffractometer with Cu Kα radiation (λ = 1.5418 Å) at a scan rate of 20° min^{-1}. Scanning electron microscopic (SEM) images were obtained by ZEISS MERLIN Compact. Grazing incidence wide-angle X-ray scattering (GIWAXS) pattern were obtained by Xeuss 3.0 (Xenocs company, France) with the incident angle of 0.5°.

The light intensity was calibrated by a certified silicon diode and the simulator irradiance was characterized by a calibrated spectrometer. The external quantum efficiency (EQE) was collected by using a QE-R Solar Cell Spectral Response Measurement System (Enli Technology Co., Ltd., Taiwan).

The current density-voltage (*J-V*) curves of photovoltaic devices were obtained by a Keithley 2400 source measure unit under AM 1.5 G illumination at 100 mW cm^{-2} using a xenon-lamp-based solar simulator (SS-F5-3A, Enli tech). The scan directions were forward (0 V → +1.2V) and reverse (+1.2 V → 0 V).

TPV and TPC measurements. A white light bias was generated from an array of diodes (Molex 180081-4320) with light intensity about 0.5 sun. A diode pumped laser (Lapa-80) was used as the perturbation source, with a pulse duration of 10 ns and a repetition frequency of 20 Hz. Voltage and current dynamics were recorded on a digital oscilloscope (Tektronix

MDO4104C), and voltages at open circuit and currents under short circuit conditions were measured over a 1 MΩ and a 50 Ω resistor, respectively.

Trap density and mobility measurements. The trap-state density N_t of control and target-1 perovskite films were performed by space-charge-limited-current (SCLC) method using a diode configuration of ITO/NiO_x/Me-4PACZ/Perovskite/Spiro-OMeTAD/MoO_x/Ag for hole and ITO/SnO_2/Perovskite/$PC_{61}BM$/BCP/Ag for electron by taking the dark current density in the range of 0–4 V and fitting the results to a space charge limited form, where the N_t was calculated according to the relation: $N_t = 2\varepsilon_0\varepsilon rVTFL/qL^2$, where V_{TFL} is the trap-filled limit voltage, ε_0 is the vacuum permittivity, and e is the electron charge, L is the thickness of the perovskite film.

4. Supporting Figures

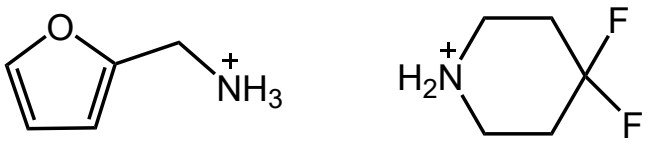

FuMA DFP

Figure S1. The chemical structures of FuMA and DFP spacers.

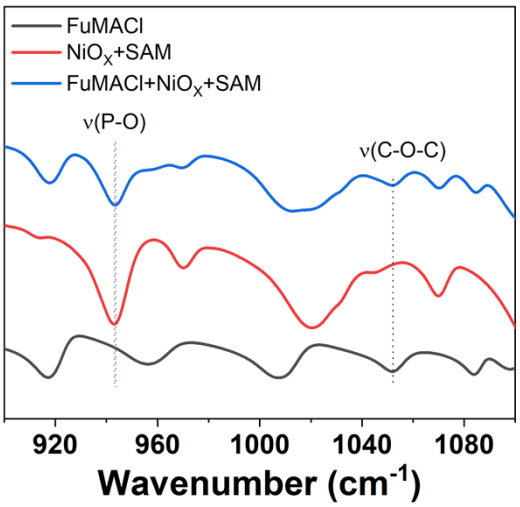

Figure S2. FTIR spectra of FuMACl, NiO_X+SAM and FuMACl (NiO_X+SAM).

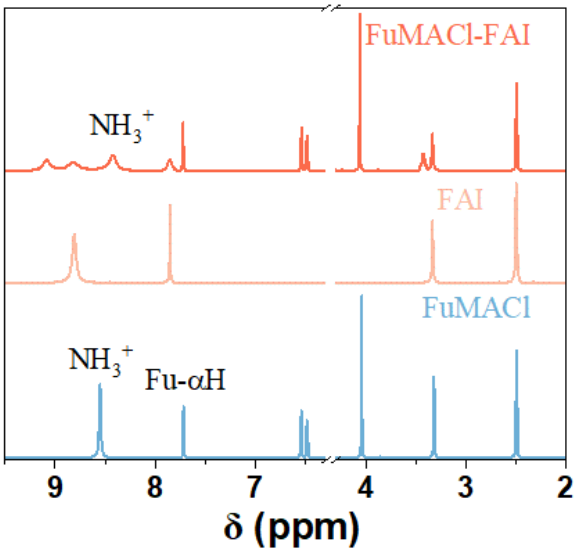

Figure S3. Chemical shift information of FuMACl, FAI and FuMACl (FAI) complex obtained from ^{1}H NMR measurements.

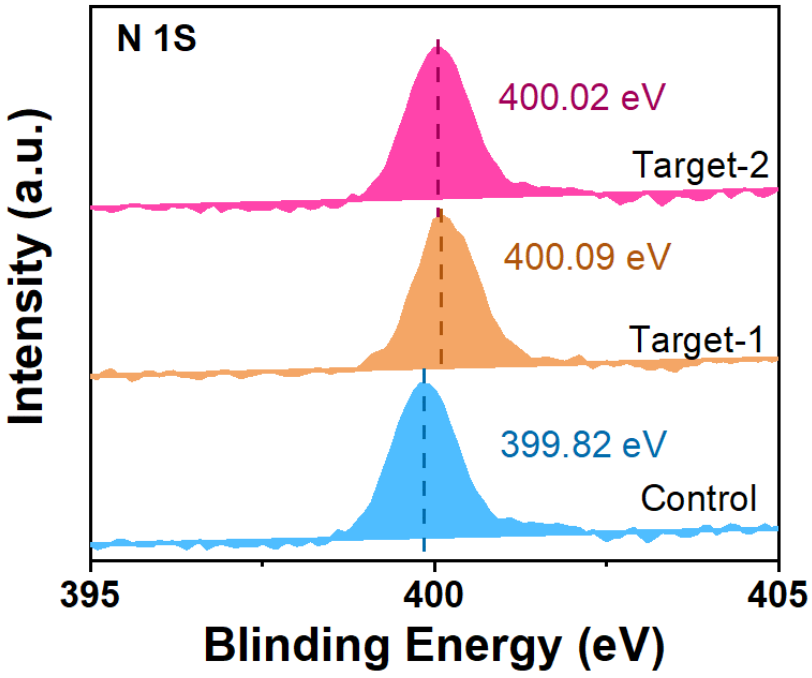

Figure S4. N 1S XPS spectra of the control, target-1 and target-2 perovskite thin film.

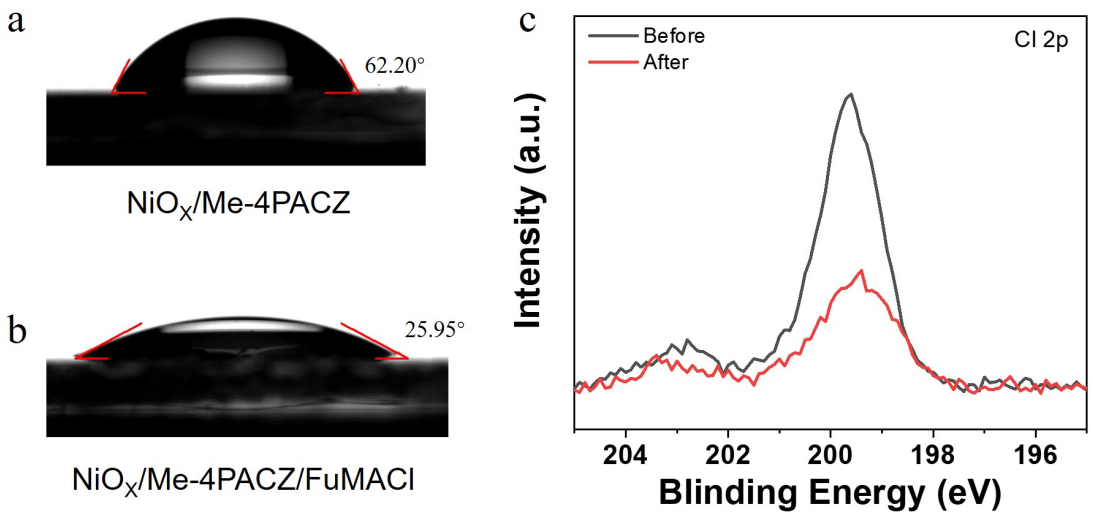

Figure S5. (a) The contact angle measurement of a DMF and DMSO (4:1) droplet on NiO_X/Me-4PACZ films. (b) The contact angle measurement of a DMF and DMSO (4:1) droplet on NiO_X/Me-4PACZ/FuMACl films. (c) XPS spectra of the ITO/NiOX/SAM/FUMACl before and after washing with DMF/DMSO (4:1, v/v).

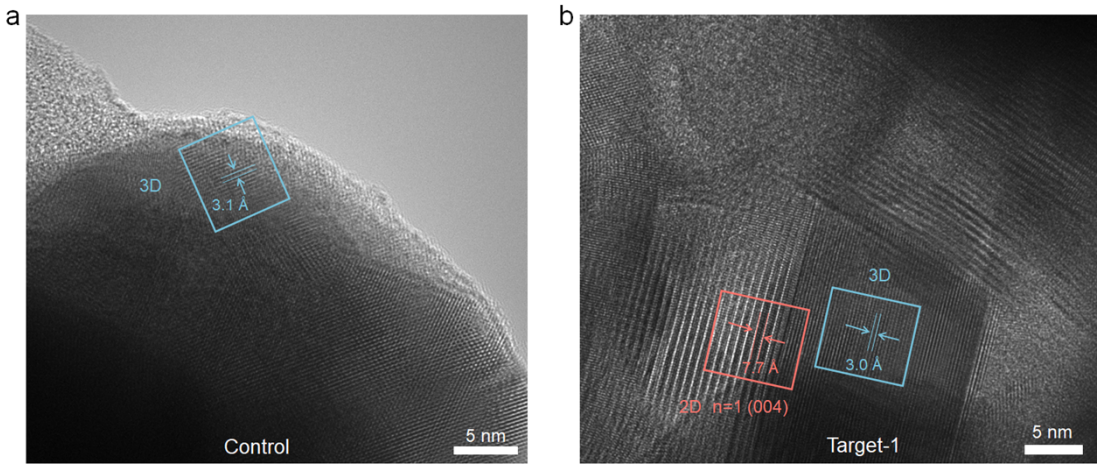

Figure S6. (a) HRTEM images of the control perovskite films. (b) HRTEM images of the target-1 perovskite films.

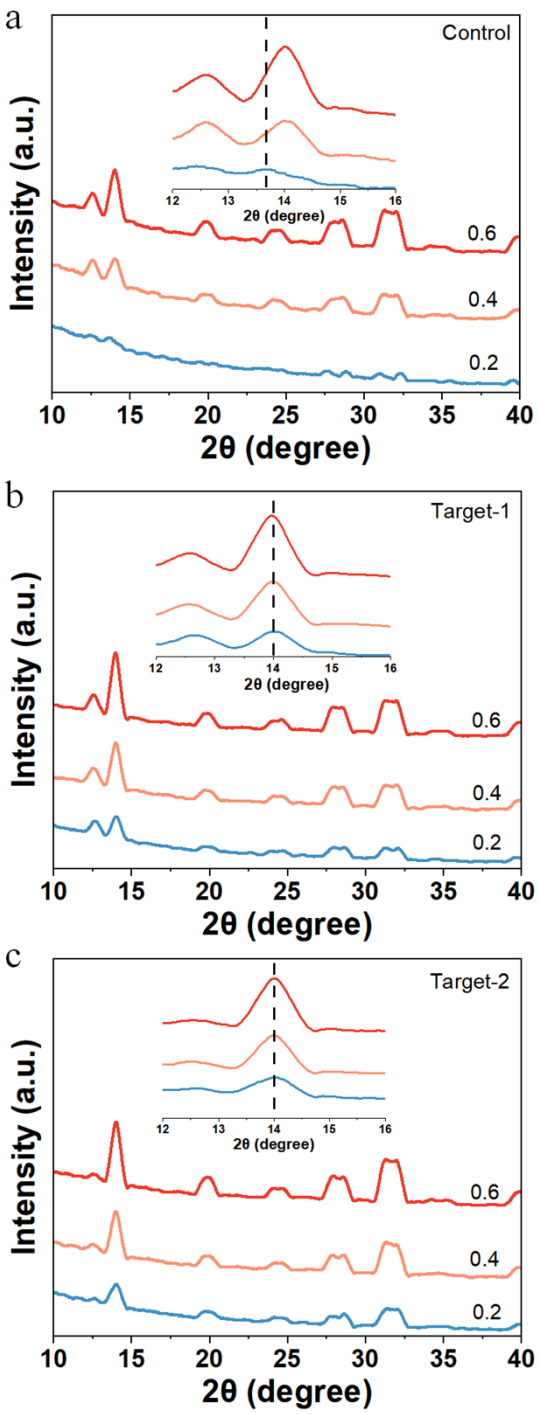

Figure S7. (a) GIXRD results of control films at different incidence angles. (b) GIXRD results of target-1 films at different incidence angles. (c) GIXRD results of target-2 films at different incidence angles.

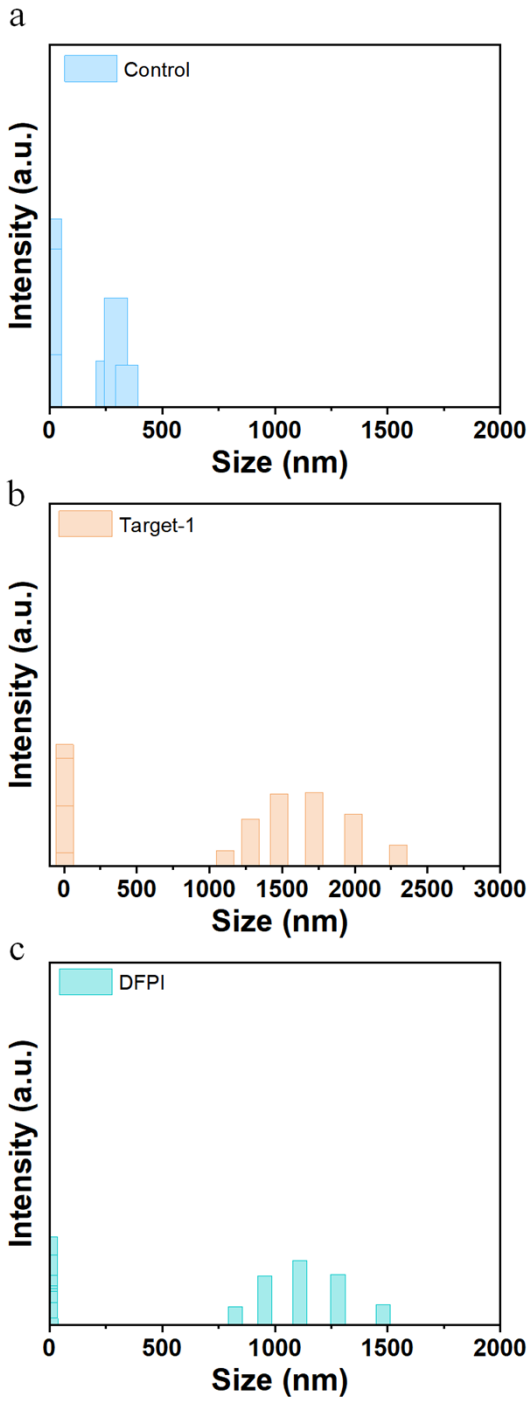

Figure S8. (a) The DLS measurements of control precursor solutions. (b) The DLS measurements of target-1 precursor solutions. (c) The DLS measurements of 4,4-Difluoropiperidine Hydroiodide (DFPI) precursor solutions.

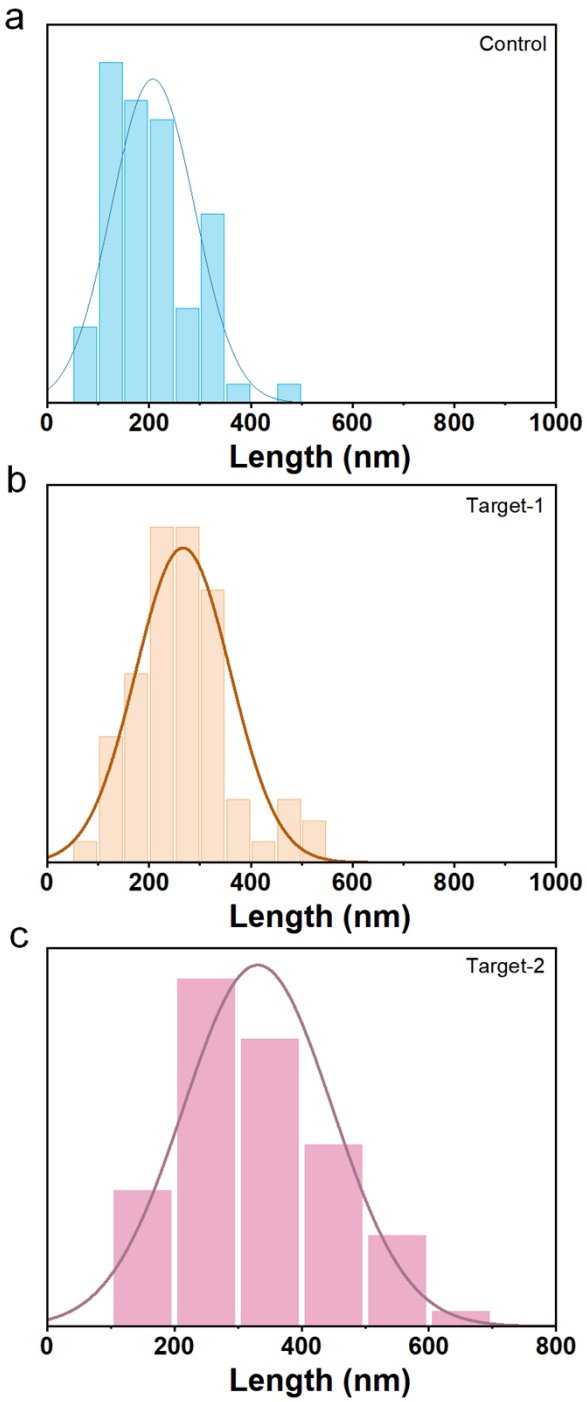

Figure S9. (a) Grain size distribution extracted from SEM images of the control perovskite films. (b) Grain size distribution extracted from SEM images of the target-1 perovskite films. (c) Grain size distribution extracted from SEM images of the target-2 perovskite films.

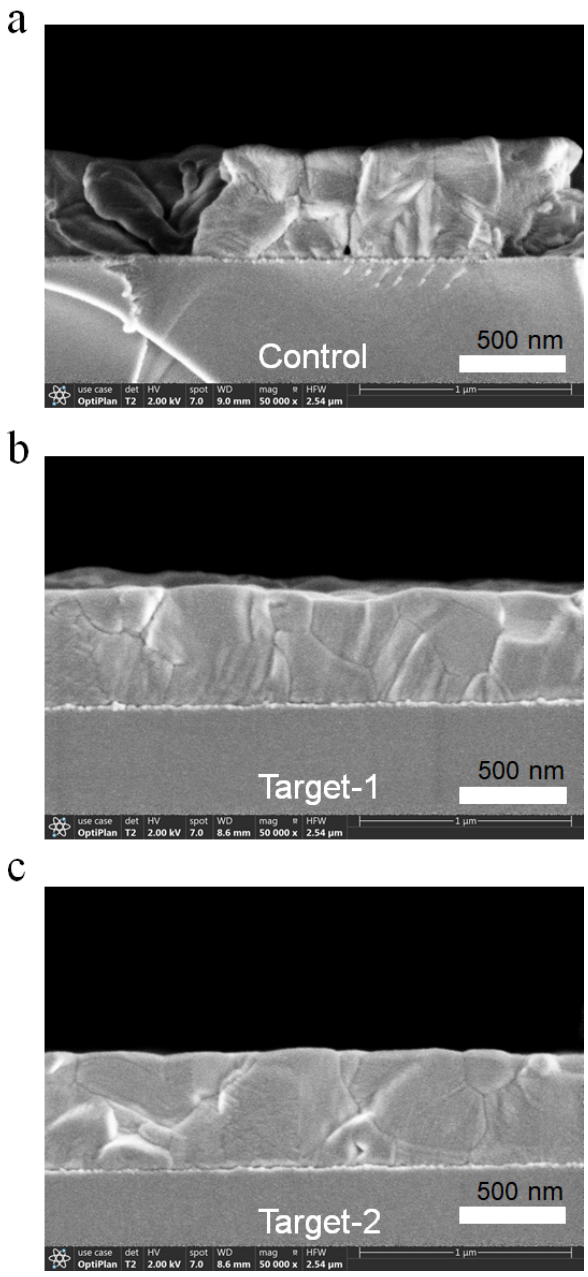

Figure S10. (a) Cross-sectional SEM of the control film. (b) Cross-sectional SEM of the target-1 film. (c) Cross-sectional SEM of the target-2 film.

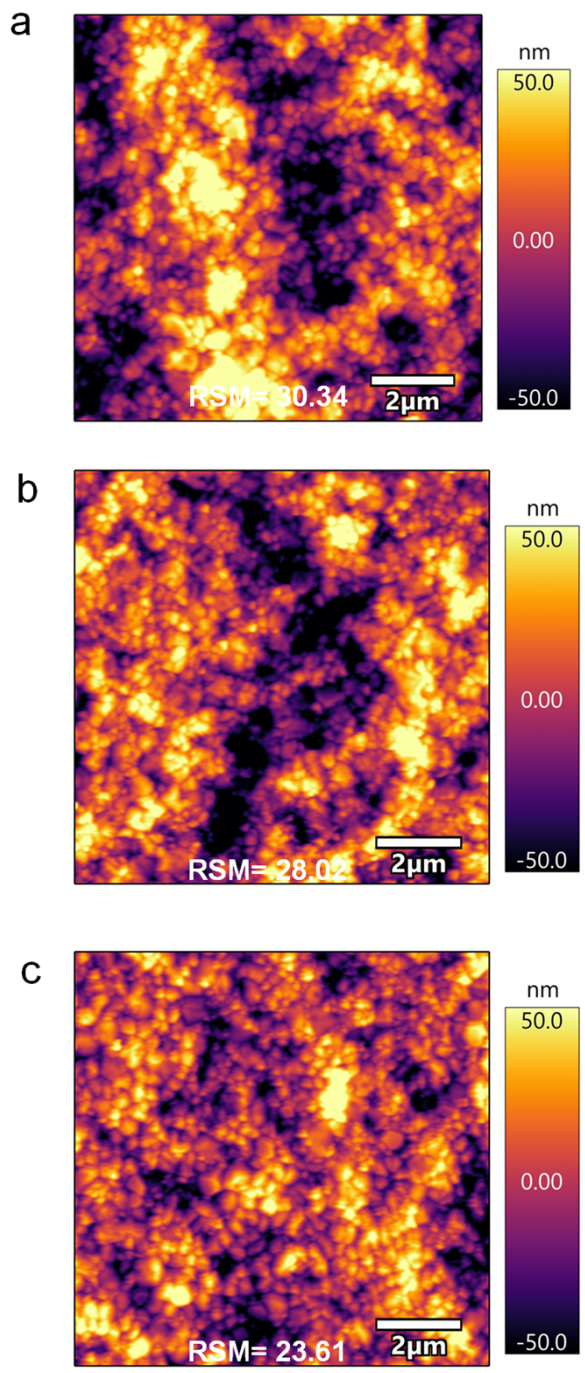

Figure S11. (a) Taping-mode AFM height images of control perovskite films. (b) Taping-mode AFM height images of target-1 perovskite films. (c) Taping-mode AFM height images of target-2 perovskite films.

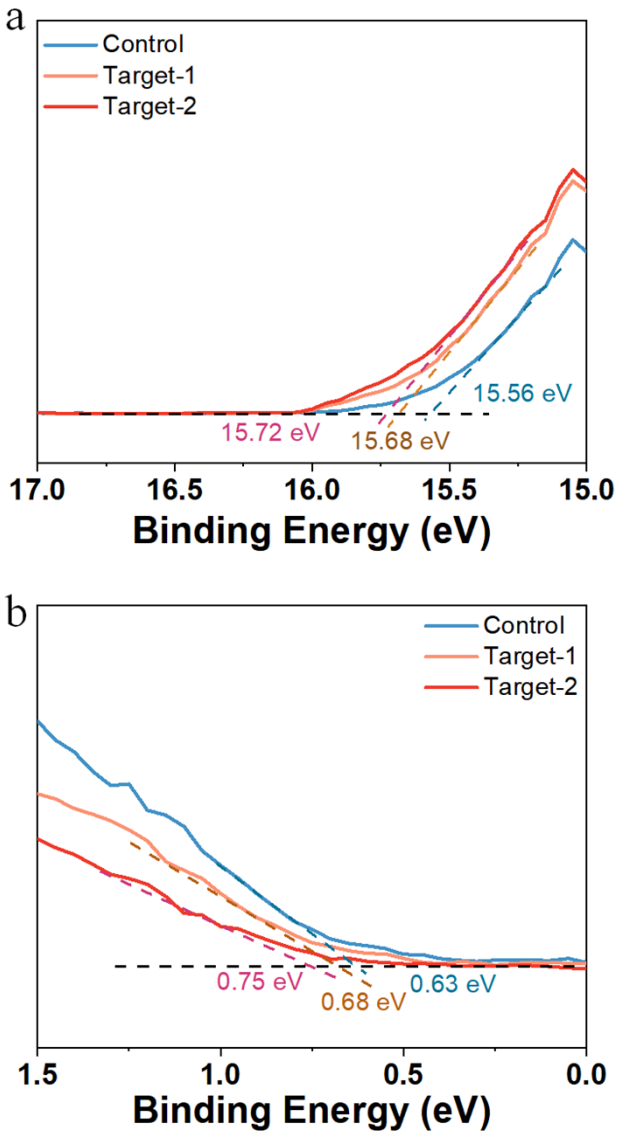

Figure S12. (a) Secondary cutoff region of UPS for control, target-1 and target-2 films. (b) Energy difference between Fermi energy levels and VB for control, target-1 and target-2 films.

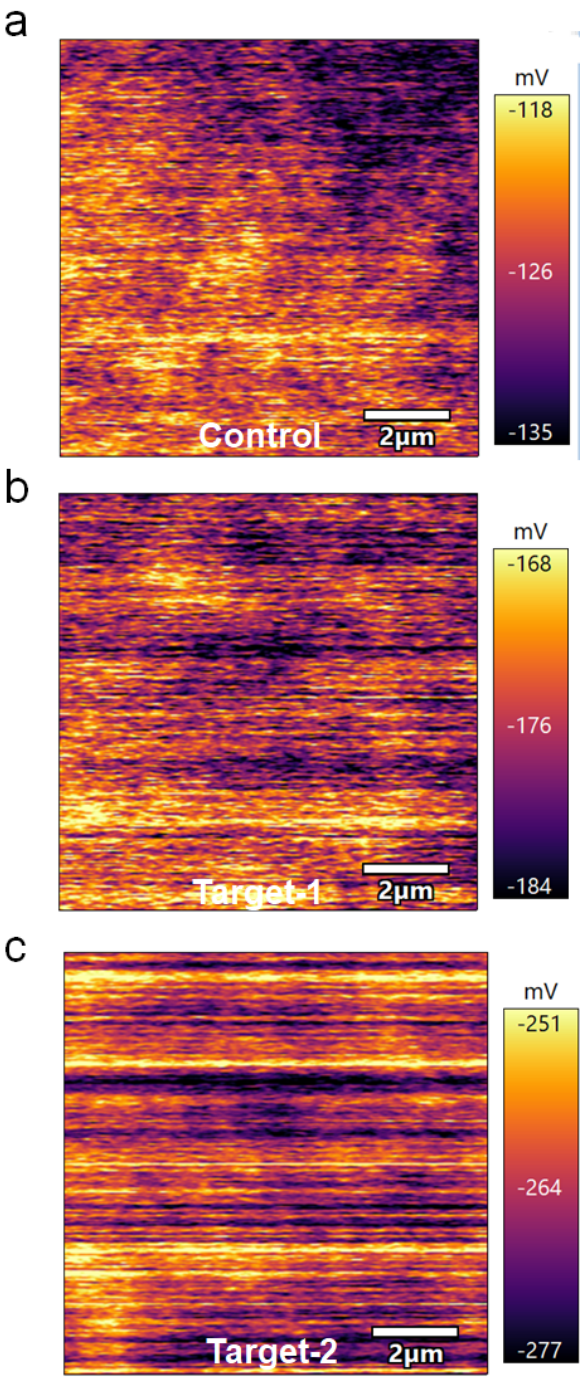

Figure S13. (a) Kelvin probe force microscopy (KPFM) surface potential images of the control film. (b) KPFM surface potential images of the target-1 film. (c) KPFM surface potential images of the target-2 film.

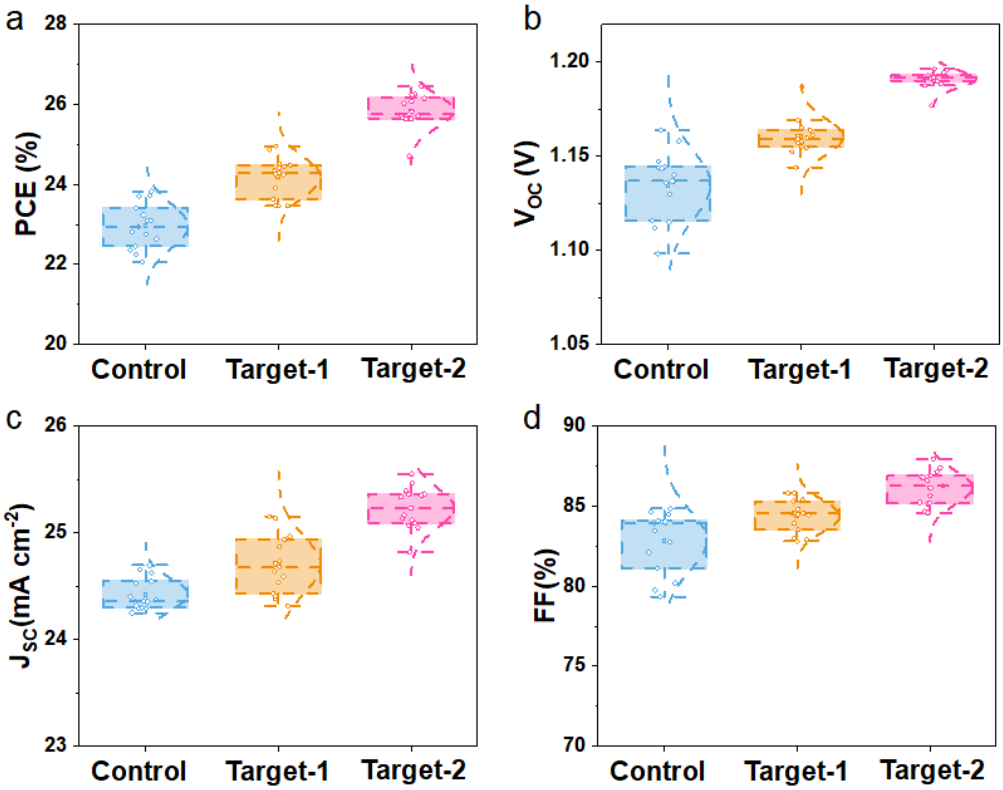

Figure S14. Statistical PCE (a) V_{OC} (b) J_{SC} (c) and FF (d) data of the corresponding devices obtained from 15 individual devices.

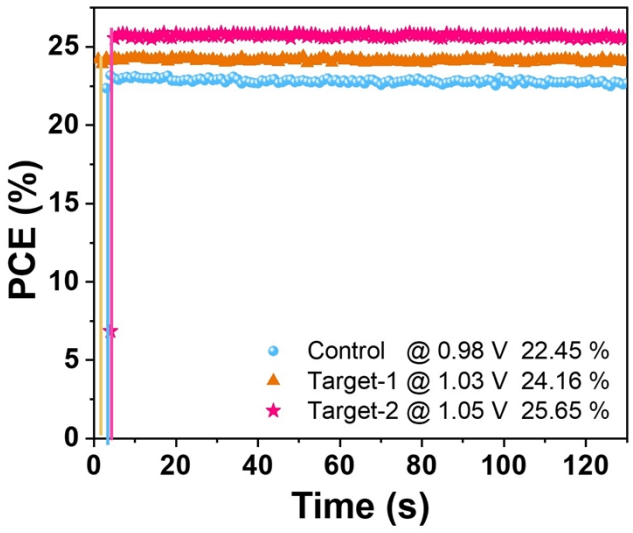

Figure S15. The reverse and forward *J-V* scan of target-2 device.

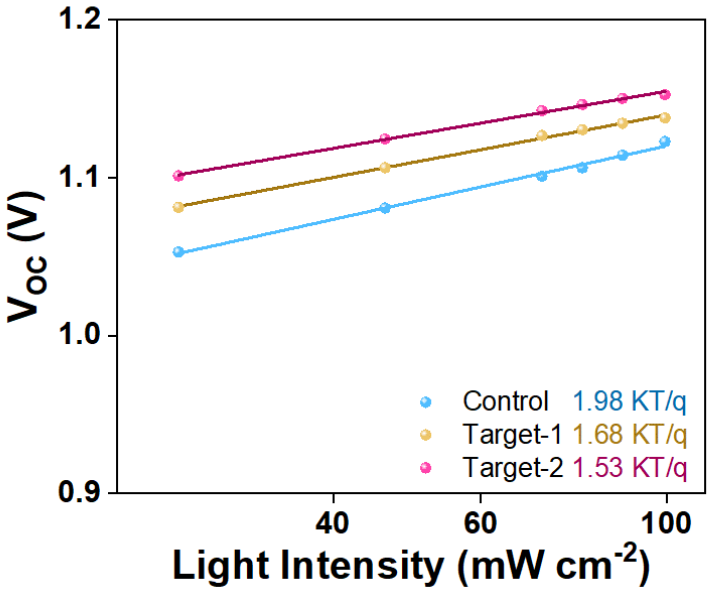

Figure S16. V_{OC} versus light intensity for the corresponding devices.

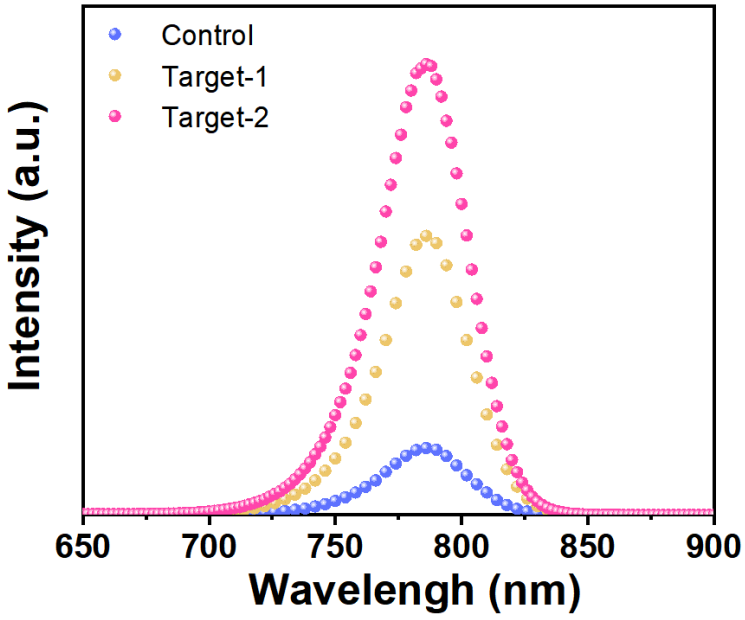

Figure S17. Steady-state PL of excited from the buried interface for the control, target-1 and target-2 films.

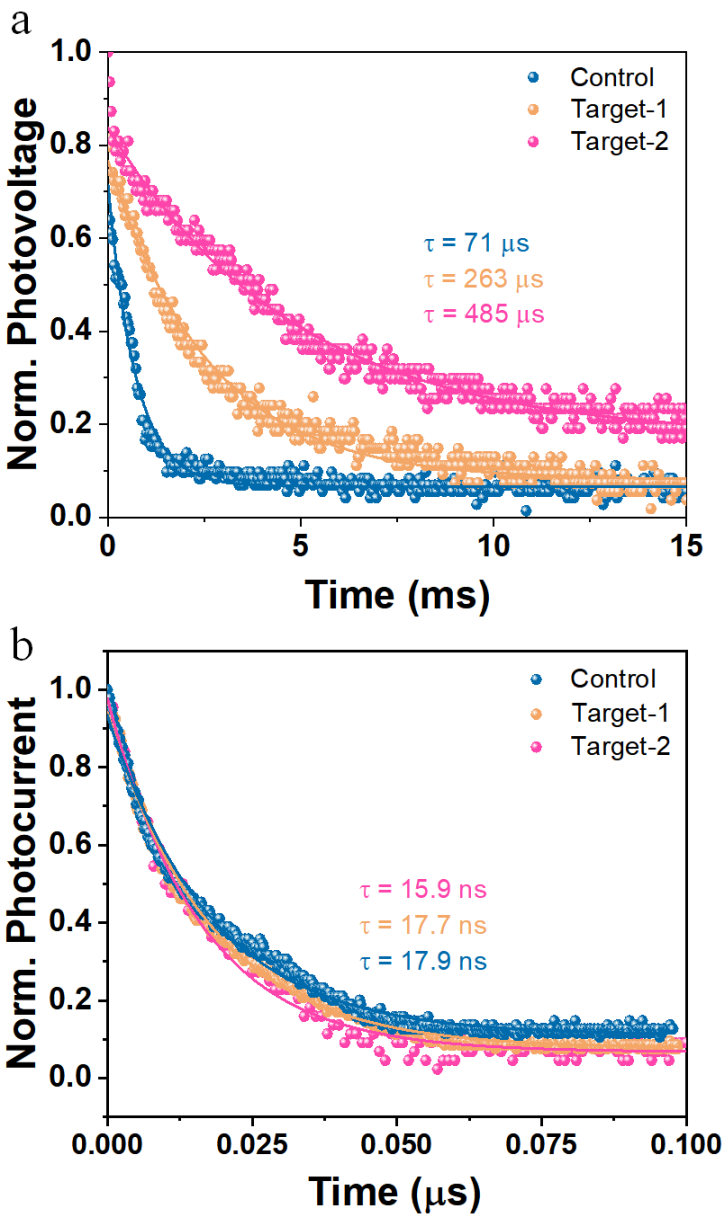

Figure S18. (a) TPV decay curves for the control target-1 and target-2 perovskite devices. (b) TPC decay curves for the control target-1 and target-2 perovskite devices.

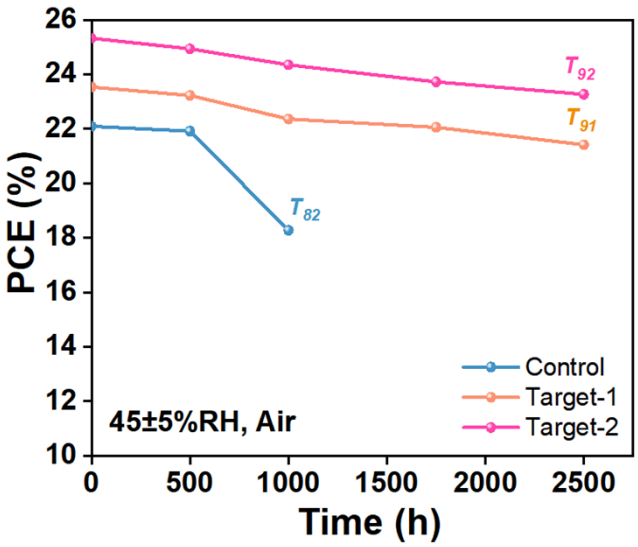

Figure S19. Ageing test of the unencapsulated devices stored in air (RH, 45 ± 5%).

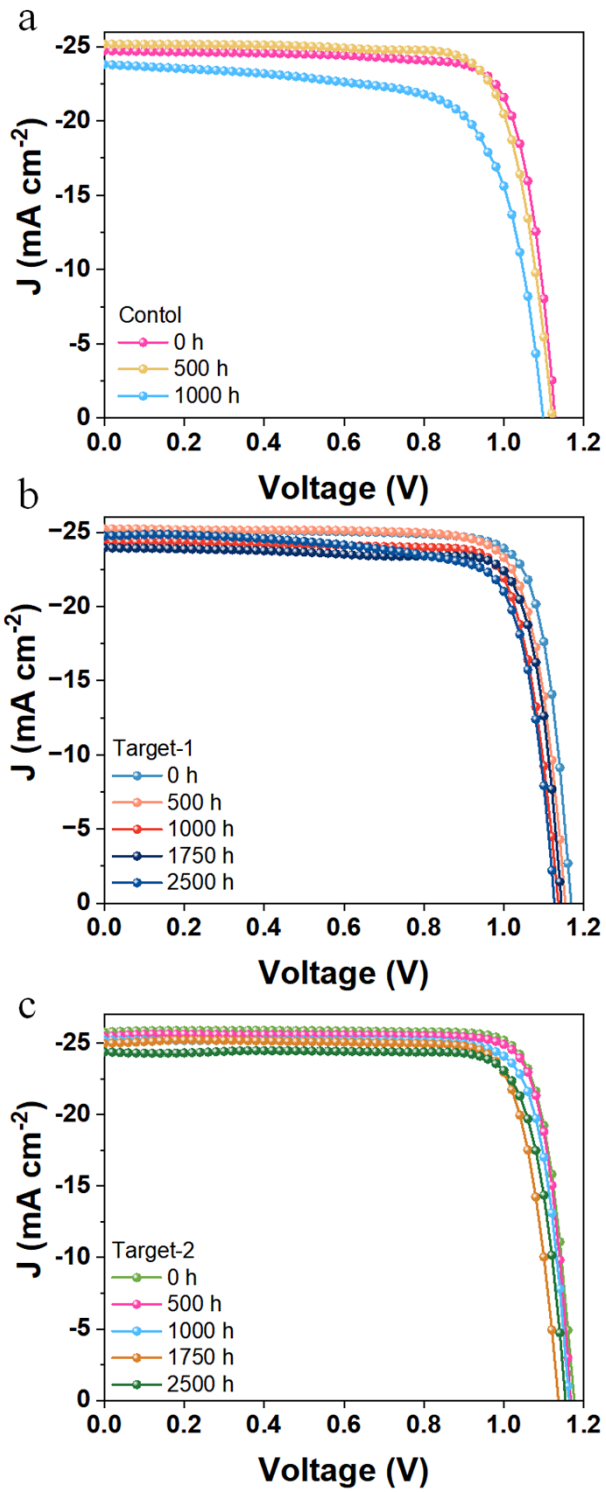

Figure S20. Aging test of the *J-V* date for unencapsulated control (a), target-1 (b) and target-2 (c) devices stored in air (RH, 45±5 %).

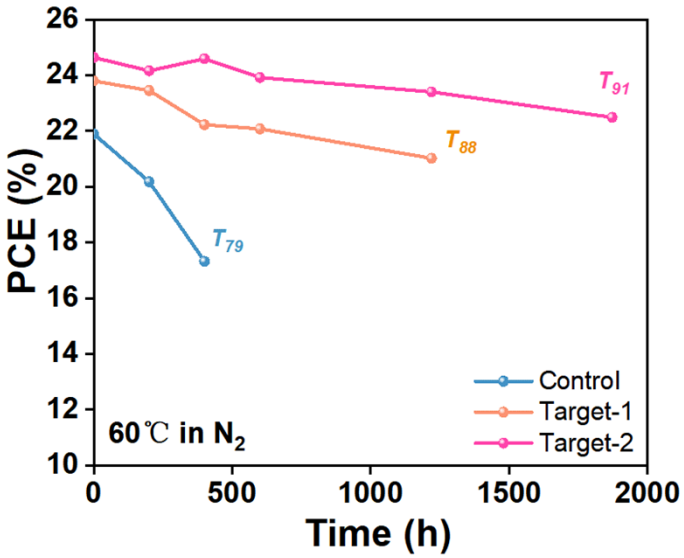

Figure S21. Aging test of the unencapsulated devices under constant heating at 60 °C in N_2.

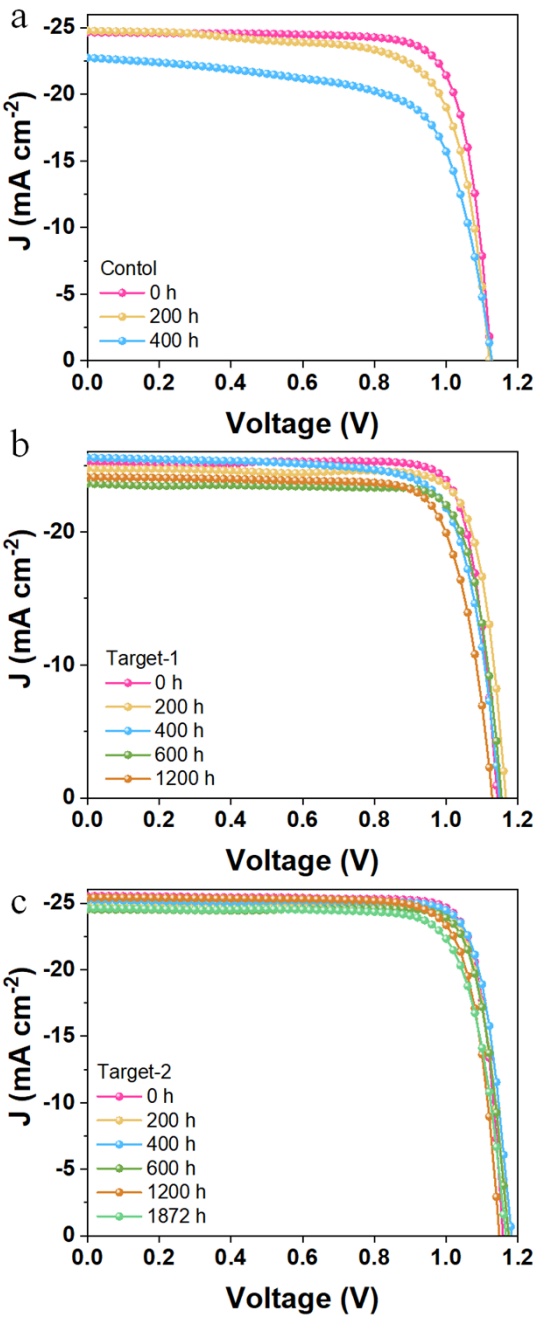

Figure S22. (a) The *J-V* of device stability based on ageing test of the unencapsulated control devices under constant heating at 60 °C in N_2. (b) The *J-V* of device stability based on ageing test of the unencapsulated target-1 devices under constant heating at 60 °C in N_2. (c) The *J-V* of device stability based on ageing test of the unencapsulated target-2 devices under constant heating at 60 °C in N_2.

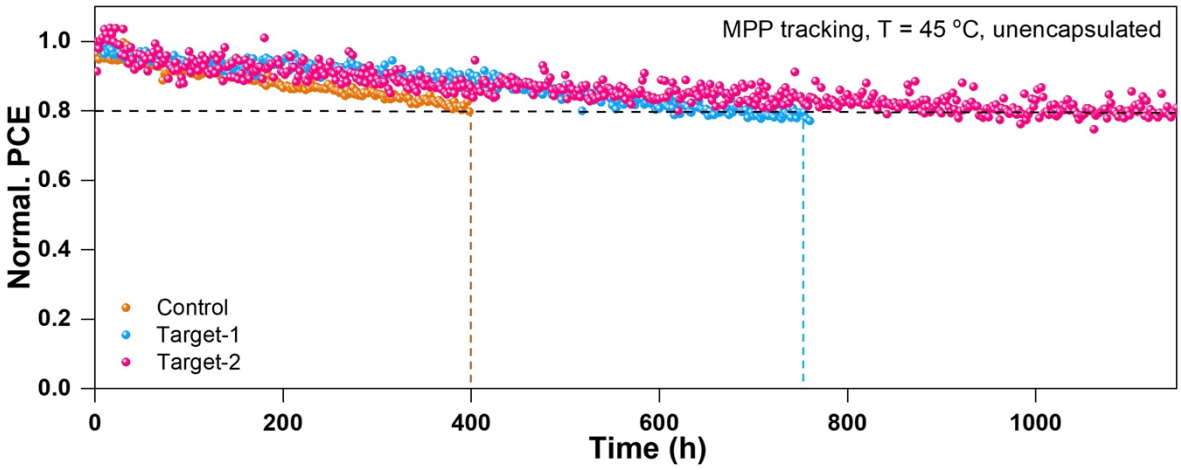

Figure S23. MPP tracking of the unencapsulated devices unstimulated AM1.5 illumination, 100 mW cm^{-2} in nitrogen atmosphere at 45 ^{o}C.

5. Supporting Tables

Table S1. Photovoltaic parameters of devices based on ITO/PTAA and ITO/2PACZ substrates with and without FuMACl layer.

HTL	FuMACl	V_{OC} (V)	J_{SC} (mA cm^{-2})	FF (%)	PCE (%)
PTAA	w/o	1.127	23.83	81.03	21.77
	w/	1.162	24.27	81.19	22.90
2PACZ	w/o	1.119	24.09	77.20	20.82
	w/	1.147	24.69	80.59	22.83

Table S2. Photovoltaic parameters of control, target-1 and target-2 devices.

Devices	Scan	V_{OC} (V)	J_{SC} (mA cm^{-2})	FF (%)	PCE (%)
Control	Reverse	1.140	24.62	84.85	23.82 (22.82±1.0)
	Forward	1.125	24.60	82.53	22.85
Target-1	Reverse	1.163	25.01	85.30	24.82 (24.12±0.7)
	Forward	1.160	24.94	83.21	24.09
Target-2	Reverse	1.192	25.16	86.79	26.03 (25.76±0.3)
	Forward	1.192	25.18	85.56	25.68

Table S3. Photovoltaic parameters of target-1 with different concentrations FuMACl.

Devices	Scan	V_{OC} (V)	J_{SC} (mA cm^{-2})	FF (%)	PCE (%)
0.5 mg/mL	Reverse	1.157	24.60	84.69	24.10
	Forward	1.143	24.52	83.47	23.40
1 mg/mL	Reverse	1.163	25.01	85.30	24.82
	Forward	1.160	24.94	83.21	24.09
2 mg/mL	Reverse	1.172	24.94	80.83	23.60
	Forward	1.164	24.94	76.30	22.13

Table S4. Photovoltaic parameters of module device (5×5 cm^2).

Devices	Scan	V_{OC} (V)	J_{SC} (mA cm^{-2})	FF (%)	PCE (%)
Module device (10.80 cm^{-2})	Reverse	6.91	4.25	78.17	22.89
	Forward	6.90	4.25	74.04	21.62

Table S5. Summary of photovoltaic parameters of WBG target devices.

Devices	Scan	V_{OC} (V)	J_{SC} (mA cm^{-2})	FF (%)	PCE (%)
WBG control device	Reverse	1.241	16.98	73.34	15.47
	Forward	1.245	16.27	69.21	14.06
WBG target device	Reverse	1.345	16.74	83.68	18.88
	Forward	1.331	16.69	83.68	18.59

References

[1] P. Zhu, D. Wang, Y. Zhang, Z. Liang, J. Li, J. Zeng, J. Zhang, Y. Xu, S. Wu, Z. Liu, X. Zhou, B. Hu, F. He, L. Zhang, X. Pan, X. Wang, N.-G. Park, B. Xu, *Science* **2024**, 383, 524.